Ru-doped Bi_2O_3 with rich oxygen vacancy for enhanced photocatalytic nitrogen reduction

Qianyu Chu, Guangming Ren, Xiangchao Meng

PII: S0925-8388(24)05029-1

DOI: https://doi.org/10.1016/j.jallcom.2024.178441

Reference: JALCOM178441

To appear in: *Journal of Alloys and Compounds*

Received date: 2 November 2024
Revised date: 31 December 2024
Accepted date: 31 December 2024

Please cite this article as: Qianyu Chu, Guangming Ren and Xiangchao Meng, Ru-doped Bi_2O_3 with rich oxygen vacancy for enhanced photocatalytic nitrogen reduction, *Journal of Alloys and Compounds,* (2025) doi:https://doi.org/10.1016/j.jallcom.2024.178441

Ru-doped Bi_2O_3 with rich oxygen vacancy for enhanced photocatalytic nitrogen reduction

Qianyu Chu[1], Guangming Ren[1,2] and Xiangchao Meng[1*]*

[1]Key Laboratory of Marine Chemistry Theory and Technology (Ministry of Education), College of Chemistry & Chemical Engineering, Ocean University of China, Qingdao, Shandong, 266100, China.

[2]State Key Laboratory Base of Eco-Chemical Engineering, College of Chemical Engineering, Qingdao University of Science & Technology, Qingdao, 266042, China

**Corresponding authors, E-mail: mengxiangchao@ouc.edu.cn (X.M.)*

Abstract

Photocatalytic nitrogen reduction is promising for green ammonia synthesis. Nevertheless, the photocatalytic activity is critically limited by high carriers' recombination and poor adsorption/activation of dinitrogen molecules. Herein, a rapid Joule heating method was applied to synthesize Bi_2O_3 with rich oxygen vacancies. This leads to a high separation rate of photogenerated carriers. Accordingly, the photocatalytic ammonia synthesis rate of Ru-Bi_2O_3 was higher than pristine Bi_2O_3, reaching 32.9 μmol g^{-1} h^{-1}. Characterization and density functional theory confirmed that metal-support interactions between Bi_2O_3 and Ru lead to charge redistribution. This will lower the energy barrier for the rate-determining step of nitrogen hydrogenation, further confirming the applicability of the alternating nitrogen fixation pathway to this process.

1. Introduction

Since N_2 has a highly stable non-polarizable strong N≡N bond (945 kJ mol^{-1}), ammonia is industrially produced through the Haber-Bosch process operating at high temperature and high pressur[1-3]. Recently, photocatalytic nitrogen reduction reaction (NRR) has been recognized as an ideal green nitrogen fixation pathway owing to its ability to directly utilize natural resources such as solar energy, and eliminate environmental pollution at the source[4]. Despite the extensive research that has been carried out, photocatalytic NRR faces the following challenges: insufficient redox potential, negative nitrogen affinity energy, and high recombination of photogenerated carriers and holes[5]. It has been found that the antibonding π* orbitals in N_2 can accept the electrons, while the bonding orbitals feed electrons back to the catalyst, thus weakening the N≡N bond and making N_2 easy to activate [6]. Therefore, the ideal photocatalysts should have suitable active sites and a strong electron back-donation capacity, which will facilitate the activation of nitrogen by the catalyst [7].

At present, a wide range of photocatalysts have been designed for NRR. Among them, bismuth-based semiconductors are one of the most promising photocatalysts[8]. Typically, the bismuth acts as a p-block element to perform π back-donation to weaken the nitrogen-nitrogen triple bond[9-11]. Typical bismuth based semiconductors are $BiVO_4$[12], Bi_2WO_6[13], BiOX (X=Cl, Br, I)[14], *etc.* Liu et al. synthesized $Bi(OH)_3$ with good visible light responsivity and abundant alkaline groups, thus facilitating the efficiency of the photocatalytic reduction reaction[15]. Bi_2O_3 is also a promising photocatalyst for immobilizing N_2 due to its stable atomic structure and pronounced narrow forbidden band gap[16-20].

The doping of precious metals is one of the most effective modification methods. It can increase the active sites of the reactants and increase the active sites of the reactants. The doping energy level of the trap of photogenerated carriers can be formed by doping precious metals into the semiconductor catalyst. Thus, the electron-hole recombination is effectively suppressed, and the photocatalytic activity is improved[21]. Ruthenium is presently receiving great interest owing to its high catalytic activity. Because the metal-support interaction (MSI) of Ru significantly affects the reactivity of the catalyst in

photocatalysis. Wang et al. synthesized Ru@MIL125/MnO_x composite catalysts using a hydrothermal method[22]. According to the characterization results, Ru served as a reactive site for photocatalytic nitrogen reduction, which can capture electrons and promote photogenerated electron transfer, thus effectively reducing electron and hole complexation. Therefore, the formation of ionic or covalent bonds between the loaded metal and the support helps to improve the stability of the metal, thus effectively regulating the electronic structure and reducing the reaction energy barrier[23-26]. Compared with the traditional heating method, the rapid Joule heating method can directly convert electrical energy into thermal energy, thus improving heating efficiency. Zhao et al. induced the deposition of Pt clusters onto C_3N_4 by the rapid Joule heating method, leading to the formation of electron-rich active Pt sites[27]. By comparing the samples prepared by the conventional heating method, it was found that the rapid Joule heating method had a shorter preparation time and more active sites. The rapid Joule heating method reduces the active sites' overoxidation reaction during prolonged heating, and rapid cooling also leads to structural deformation and defect formation, thus providing abundant catalytic sites. Moreover, the rapid Joule heating method also avoids the agglomeration of the metal, hence achieving a better dispersion of Ru[28].

The Ru-Bi_2O_3 with oxygen-rich vacancies was prepared by the rapid Joule heating method. Subsequently, the optimal catalysts with defective and electron-rich structures were explored by controlling the temperature and atmosphere of the rapid Joule heating method. Metal Ru-doped Bi_2O_3 also increased the photocatalytic nitrogen fixation rate to 32.9 μmol g^{-1} h^{-1} without a sacrificial agent. Therefore, based on the characterization and density functional theory (DFT) calculations, the Ru-Bi_2O_3 with abundant surface oxygen vacancies, as well as the electron-rich Ru sites both provided sufficient chemisorption and active sites for N_2. The Bi-O-Ru site is the optimized adsorption site to reduce the energy potential of the rate-limiting step. The reaction mechanism was then explored and discussed.

2. Experimental

2.1 Preparation of Bi_2O_3 and Ru-Bi_2O_3 catalysts

Preparation of $Bi(OH)_3$: Firstly, 1 mmol of $Bi(NO_3)_3·5H_2O$ was ultrasonically dispersed in 30 mL of deionized water, and then the pH of the $Bi(NO_3)_3·5H_2O$ suspension was adjusted to 10 using KOH. After stirring at room temperature until the mixture was homogeneous, it was transferred to a 100-mL Teflon-lined stainless-steel autoclave and reacted at 150°C for 12 h. The samples obtained were washed and separated. The resulting white precipitate was collected and dried in a desiccator at 80°C for 12 h to synthesize a $Bi(OH)_3$ sample.

Preparation of Bi_2O_3: The rapid Joule heating method applied high pulse voltage and strong pulse current to $Bi(OH)_3$ instantaneously under different atmospheres to bring it to the selected temperature. The sample was heated at a high temperature, and the yellow solid Bi_2O_3 was synthesized.

Preparation of Ru-Bi_2O_3: $Bi(OH)_3$ samples with different Ru contents were synthesized by the impregnation method. First, various amounts of $RuCl_3·3H_2O$ solution (10 g/L) were added to deionized water and sonicated homogeneously. Then, $Bi(OH)_3$ was dispersed in the above solution and heated in a water bath for 4 h at 60°C. The synthesized solution was subsequently centrifuged, dried and collected as x wt% Ru-$Bi(OH)_3$ (x = 0, 0.50, 0.75, 1.0, 1.25, 1.50), where x denotes the mass percentage of the doped metal element. Ru-$Bi(OH)_3$ was heated at different temperatures (500℃, 600℃, 700℃, 800℃) and different atmospheres (N_2, Ar, H_2/Ar and Air) using the rapid Joule heating method. A high pulse voltage and a strong pulse current were instantaneously applied to Ru-$Bi(OH)_3$ to reach the specified temperature rapidly. A gray-black powder was synthesized, and the product was named Ru-Bi_2O_3. Bi_2O_3 of other metals were prepared using the same impregnation method, and the products were labelled as Pt-Bi_2O_3 and Pd-Bi_2O_3.

2.2 Photocatalytic N_2 fixation measurement

The photocatalytic nitrogen fixation performance of the catalysts was tested. The steps were as follows: 30 mg of the photocatalyst was ultrasonically dispersed in deionized water, and a quartz reactor was filled with high-purity N_2 and continuously stirred. Recirculating water was continuously passed through the test process to maintain room

temperature and minimize thermal effects. The reaction was irradiated under a 300 W Xe lamp for 1 h. Upon completion of the reaction, 10 mL of clear reaction solution was collected by syringe and filtered. NH_4^+ concentration was quantified using Nessler's reagent spectrophotometric method.

3. Results and discussion

3.1 Morphology and chemical composition

The fabricated Ru-Bi_2O_3 and Bi_2O_3 samples were prepared by rapid Joule heating as shown in Fig. S1. Firstly, $Bi(OH)_3$ was prepared by a hydrothermal method, while different amounts of Ru were doped into $Bi(OH)_3$ by impregnation method. Then, Ru-Bi_2O_3 was synthesized by the rapid Joule heating method at different temperatures and under different atmospheres. The morphology and microstructure of the samples were analyzed by SEM and TEM. The morphology of Bi_2O_3 was observed to be a flower-shaped structure consisting of thin flakes with a size of about 1-2 μm, with a rough and compact surface (Fig. 1a). As can be seen from Fig. 1b, the morphology of Ru-doped Bi_2O_3 is similar to Bi_2O_3 in the form of irregular nanoflower clusters. The rough and compact surface may be attributed to the high-temperature treatment by the rapid Joule heating method, which avoids the structural collapse and aggregation process[29]. Figs. 1c and 1d show the TEM and HRTEM images of Ru-Bi_2O_3. The lattice spacing of 0.31 nm as measured corresponded to the (1 2 1) face of Ru-Bi_2O_3, in agreement with the XRD results (Fig. 2a)[30-31]. It was also found that significant blurring and disorder appeared in the middle of the lattice stripes of the Ru-Bi_2O_3 photocatalyst suggesting that the surface structure of Ru-Bi_2O_3 was disrupted by the rapid Joule heating treatment, followed by the formation of surface oxygen vacancies[16].

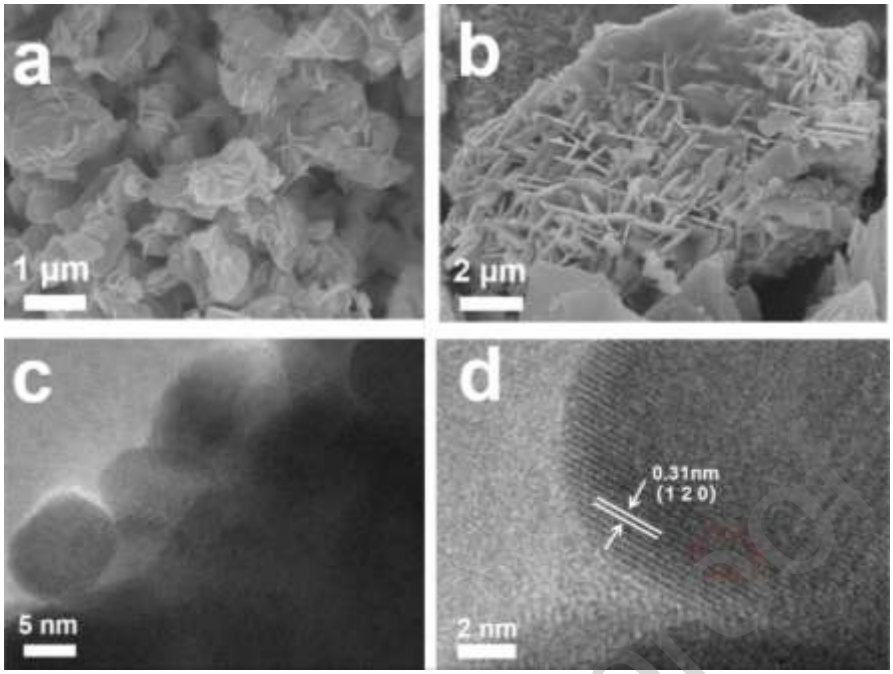

Fig. 1. (a-b) SEM images of Bi_2O_3 and Ru-Bi_2O_3, (c-d) TEM and HRTEM images of Ru-Bi_2O_3.

The crystal structure of the catalysts was characterized by X-ray diffraction (XRD). The XRD patterns of Bi_2O_3 and Ru-Bi_2O_3 prepared by the rapid Joule heating was shown (Fig. 2a), and their characteristic peaks at 24.7°, 25.8°, 27.0°, 27.5°, 28.1°, 33.1°, 33.3°, and 46.5°corresponded to the (1 0 2), (1 1 2), (-1 1 1), (1 2 0), (0 1 2), (1 2 2), (2 0 2), and (0 4 1) planes of Bi_2O_3 (JCPDS No. 72-0398), respectively. The patterns of as-prepared catalyst had a slight angular shift from the standard card, mainly due to lattice distortion caused by the rapid Joule heating method[32]. The crystal structure of Ru-Bi_2O_3 was affected by Ru doping compared to Bi_2O_3. It can be observed that the diffraction peak at 27.5° was shifted by 0.21° to a larger diffraction angle after Ru doping. This might be because the ruthenium ionic radius (0.62 Å) introduced through doping was smaller than the bismuth ionic radius (1.03 Å). This led to the contraction of the Bi_2O_3 lattice, which resulted in a smaller crystal plane spacing, indicating the successful doping of Ru into Bi_2O_3[16]. No characteristic peaks were observed for the Ru compounds, suggesting that the effects of Ru doping and oxygen vacancies on the Bi_2O_3 crystal structure were negligible.

X-ray photoelectron spectroscopy (XPS) was used to investigate the interaction between Bi_2O_3 and Ru. The XPS survey spectrum showed the presence of Bi, Ru and O as well as amorphous carbon on the surface of Ru-Bi_2O_3 (Fig. S2). After the

introduction of Ru into Bi_2O_3, the Ru 3d spectrum and the Ru 3p spectrum can be clearly detected in Fig. 3b, indicating the successful doping of Ru. In Ru 3p, the peak at 465.38 eV corresponds to the Ru^{4+} material, while 461.18 eV can be attributed to Ru^0. This suggested that Ru-Bi_2O_3 produced both Ru^0 and Ru^{4+} in the rapid Joule heating method and H_2/Ar reducing atmosphere (Fig. 2b). While 284.81 eV and 288.22 eV in the Ru 3d plot correspond to the carbon peaks in bismuth oxide C 1s, where Ru $3d_{3/2}$ can overlap with C 1s (284.8 eV), the other peak with higher binding energy (286.45 eV) can be attributed to the Ru^{4+} substance, which further suggested the presence of Ru^{4+} in the photocatalytic process of Ru-Bi_2O_3 (Fig. S3). It also reflected the possibility that Ru may form chemical bonds with surface oxygen on the Bi_2O_3 surface since the charge density of Ru is only affected by the interfacial charge transfer that occurs on Bi_2O_3[33]. Due to the photoelectron emission from Bi^{3+}, bimodal peaks corresponding to the Bi^{3+} of pristine Bi_2O_3 were found at 158.75 eV and 164.06 eV (Fig. 2c). This indicated that it was the oxidation state of Bi^{3+} that is present and not the oxidation state of other Bi[34]. Spin-orbit splitting and spectrally heavy states at 5.3 eV were characteristic of Bi^{3+} in oxide environments[35]. There was a significant peak at 529.55 eV corresponding to Bi-O-Bi, red-shifted after Ru doping, probably due to the bonding of Ru instead of Bi. Compared with pristine Bi_2O_3, the binding energies of Bi $4f_{7/2}$ and Bi $4f_{5/2}$ in the Ru-Bi_2O_3 structure were reduced to 158.9 and 164.2 eV, respectively. This may be due to the change in the electronic structure of the Bi_2O_3 samples due to doping with Ru [36-37]. As shown in Fig. 2d, O 1s can be separated into lattice oxygen (529.55 eV), oxygen vacancy (531.20 eV), and surface chemisorbed oxygen (532. 31 eV)[38-39]. In the O 1s spectra, the peaks of both lattice oxygen and OVs were red-shifted, indicating a distortion of the lattice and verifying an increase in bonding energy during rapid Joule heating. In contrast, ruthenium doping and high-temperature treatment led to the formation of unsaturated Bi-O bonds in Bi_2O_3[16]. Defect types were further verified by EPR spectroscopy[40]. A strong signal at g = 2.003 can be found in Fig. S4, proving that the defects in Bi_2O_3 and Ru-Bi_2O_3 prepared by Joule heating are oxygen vacancies[12]. The above results indicated that high-temperature rapid heat treatment had

a significant impact in regulating oxygen species and metal organization[29].

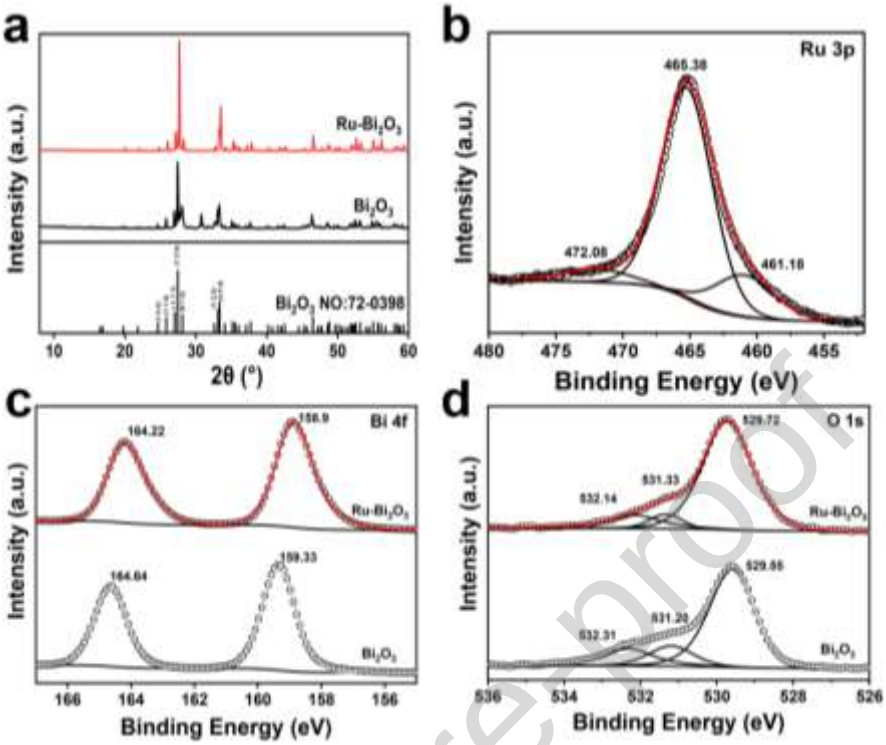

Fig. 2. (a) XRD patterns of Bi_2O_3 and Ru-Bi_2O_3, XPS spectra of (b) Ru 3p, (c) Bi 4f, (d) O 1 s.

3.2. Photocatalytic activity tests

Bi_2O_3 and Ru-Bi_2O_3 were further tested for photocatalytic ammonia synthesis. When doped with Ru, the ammonia synthesis rate of Bi_2O_3 increased from 11.1 μmol g^{-1} h^{-1} to 32.9 μmol g^{-1} h^{-1} (Fig. 3a). Thereafter, the subsequent discussion will focus mainly on the characterization of Ru-Bi_2O_3 with 1.0 wt% Ru doping under H_2/Ar atmosphere, which showed the optimum ammonia production activity of the catalysts. Furthermore, Table S1 summarized the performances of several typical photocatalytic nitrogen-fixing catalysts that have been published, suggesting that Ru-Bi_2O_3 has certain advantages[5, 24, 33, 41-43]. Meanwhile, compared with other bismuth oxide-based and bismuth-based catalysts, Ru-Bi_2O_3 can obtain good nitrogen fixation performance without the use of sacrificial agents (Table. S2)[20, 44-46]. By comparing the photocatalytic nitrogen fixation performance of Ru-Bi_2O_3 catalysts prepared by the traditional heating method (tube furnace heating method) and the rapid Joule heating method, it was found that the catalysts prepared by the rapid Joule heating method had higher performance (Fig. S5). The higher reaction rate of Ru-Bi_2O_3 may be attributed to the inhibition of the

photogenerated electron and hole complexation rate by Ru doping, which improved the photocatalytic performance. Meanwhile, the synergistic effect of Ru as both electron acceptor and electron donor with the unsaturated site on the surface of Bi_2O_3 promoted the occurrence of NRR. The highest ammonia synthesis rate was achieved for Bi_2O_3 with 1.0 wt% Ru doping (Fig. 3b). This might be due to the saturation of the surface-active sites by excess Ru, which blocked the active sites on the Bi_2O_3 reaction sites, thus reducing the photocatalytic performance. Other typical transition metals (e.g. Pd, Pt) were also doped into Bi_2O_3 using the impregnation method (Fig. 3c). As can be seen from Fig. 3d, the nitrogen fixation activity of Ru-doped Bi_2O_3 was significantly higher than that of other metal-doped Bi_2O_3. This might be due to the selective activation of nitrogen by Ru, which further enhanced the photocatalytic activity for nitrogen reduction. In addition, no other by-products such as N_2H_4 and hydrazine were detected, thus further confirming the good selectivity of Ru-Bi_2O_3. Examination of the calcination atmosphere showed that the photocatalytic nitrogen fixation performance of Ru-Bi_2O_3 was best under H_2/Ar atmosphere, which may be attributed to the fact that H_2/Ar was a reducing gas that could effectively accelerate the reduction of Ru. At the same time, Ru ions have a strong MSI effect in the inert gas Ar atmosphere[12]. As shown in Fig. 4d, Ru-Bi_2O_3 had the highest ammonia synthesis rate at 600°C, which might be due to the formation of a more stable and active structure through strong coupling between the defective portions of the Ru and Bi_2O_3 linkages at higher temperatures. In contrast, temperatures that are too high lead to excessive defects on the catalyst surface, resulting in active site rupture, which adversely affects the ammonia synthesis activity. The results indicated that the temperature and atmosphere conditions during the rapid Joule heating method have a remarkable impact on the enhancement of photocatalytic nitrogen fixation performance. Therefore, this high temperature via Joule heating played a crucial role in the modulation of the structure and chemical composition of Ru-Bi_2O_3 to achieve efficient catalytic activity and selectivity.

In addition, four consecutive measurements were performed to verify the reusability and stability of Ru-Bi_2O_3 (Fig. 3e). During the 4-hour test, no significant deactivation

of the photocatalyst was observed. Thus, it was shown that Ru-Bi_2O_3 maintains effective photocatalysis after several cycles, indicating good reproducibility. Subsequent XPS and XRD characterization of the reacted Ru-Bi_2O_3 catalysts. The stable structure of Ru-Bi_2O_3 was further demonstrated by XPS, which showed that the binding energy of the catalyst remained unchanged after light exposure and that the peaks were well-matched after the XRD reaction without collapses (Fig. S6). The ammonia synthesis activity gradually increased with light duration and the cumulative yield was 93.71 μmol g^{-1} (6 h). Additionally, the control experiment was conducted to confirm that the ammonia was indeed generated by the photocatalytic reaction of N_2 and H_2O in the samples (Fig. S7). As shown in Fig. 3f, it was found that AQE decreased with increasing wavelength of monochromatic light (0.16% at 365 nm, 0.123% at 400 nm, 0.04% at 500 nm, and 0.01% at 600 nm), which matched well with the photo-responsiveness of the DRS test for Ru-Bi_2O_3 (Fig. 4c).

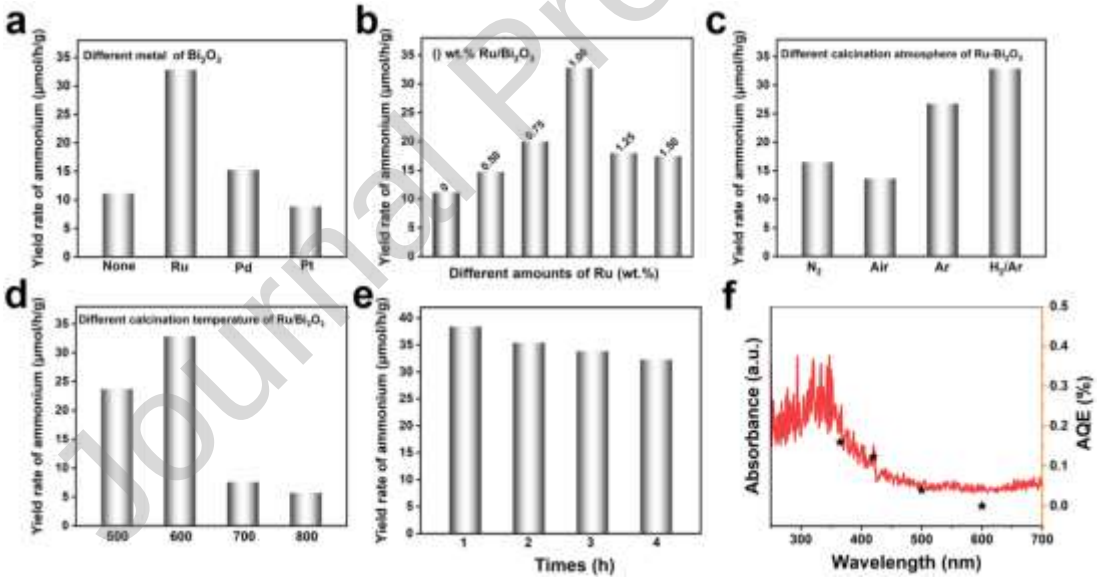

Fig. 3. (a) Photo-nitrogen fixation performance of catalysts with different doped metals, (b) different Bi_2O_3 with different Ru loading amounts, (c) different atmosphere of Ru-Bi_2O_3, (d) different calcination of Ru-Bi_2O_3, (e) Photocatalytic cycling test of Ru-Bi_2O_3 and (f) AQE (black dots) of nitrogen fixation yield on Ru-Bi_2O_3 and its optical absorption spectrum (red line).

3.3. Optical and electronic properties

The charge separation efficiency impacts photocatalytic activity, so a series of electrochemical tests were performed. As shown in Fig. 4a, the photocurrent density under light was relatively higher than that under darkness, indicating that the prepared

samples are photosensitive. The photocurrent responsiveness of Ru-Bi_2O_3 was much higher than that of Bi_2O_3, indicating a low photogenerated carrier recombination rate, a fast interfacial transport rate, and a significantly enhanced lifetime of the photogenerated electron-hole pairs[47]. Meanwhile, in the EIS spectra (Fig. 4b), the arc radius of Ru-Bi_2O_3 was much smaller than that of Bi_2O_3, suggesting that it had less charge transport resistance. Thus, it showed that Ru-Bi_2O_3 had a higher transfer capacity of interfacial charge and a lower compounding rate of photogenerated carriers, which improved the photocatalytic immobilization of N_2[14].

The study of Bi_2O_3 and Ru-Bi_2O_3 using UV-vis DRS reveals that both exhibit significant light absorption, and the absorption spectra are more intense near 400 nm, which might be related to the band gap jump of electrons. In contrast, the light absorption range of Ru-Bi_2O_3 gradually became broader, a phenomenon that can be due to the surface plasmon resonance of Ru, resulting in an apparent broad plasmon resonance absorption of Ru-Bi_2O_3 in the visible range. The corresponding Tauc plots were obtained from UV-vis DRS absorption spectra (Fig. S8) and the corresponding band gap (Eg) of Bi_2O_3 was deduced to be 2.63 eV. The doping of Ru further improved the photon absorption of Bi_2O_3 in the visible regions, which reduced its Eg to 2.38 eV. It indicated that Ru-Bi_2O_3 was more likely to produce photogenerated carriers. This phenomenon might be attributed to Ru, which increased the light absorption range and provided additional active sites for photocatalysis. Meanwhile, based on the VB-XPS plots, the E_{VB} values of Bi_2O_3 and Ru-Bi_2O_3 were obtained as 1.10 eV and 0.74 eV, respectively (Fig. S9). The calculated E_{CB} values for Bi_2O_3 and Ru-Bi_2O_3 are -1.54 eV and -1.66 eV, respectively (Fig. 4d). It might be due to the introduction of Ru as well as defects generated at high temperatures, which result in a rise in the valence band value and a narrowing of the bandgap width[48]. This was favorable for the photogenerated carriers to increase the transmission rate and separation efficiency[49]. Therefore, after Ru-Bi_2O_3 irradiation, the electrons were excited to jump to the conduction band, which suppresses the recombination rate of photogenerated carriers. More importantly, the calculated CB potentials of Bi_2O_3 and Ru-Bi_2O_3 were

thermodynamically more beneficial reactions compared to the reduction potential of N_2/NH_3 (-0.05 eV)[50]. Moreover, the Ru-doped CB was more negative and thermodynamically more favorable, resulting in a better ammonia production activity of Ru-Bi_2O_3.

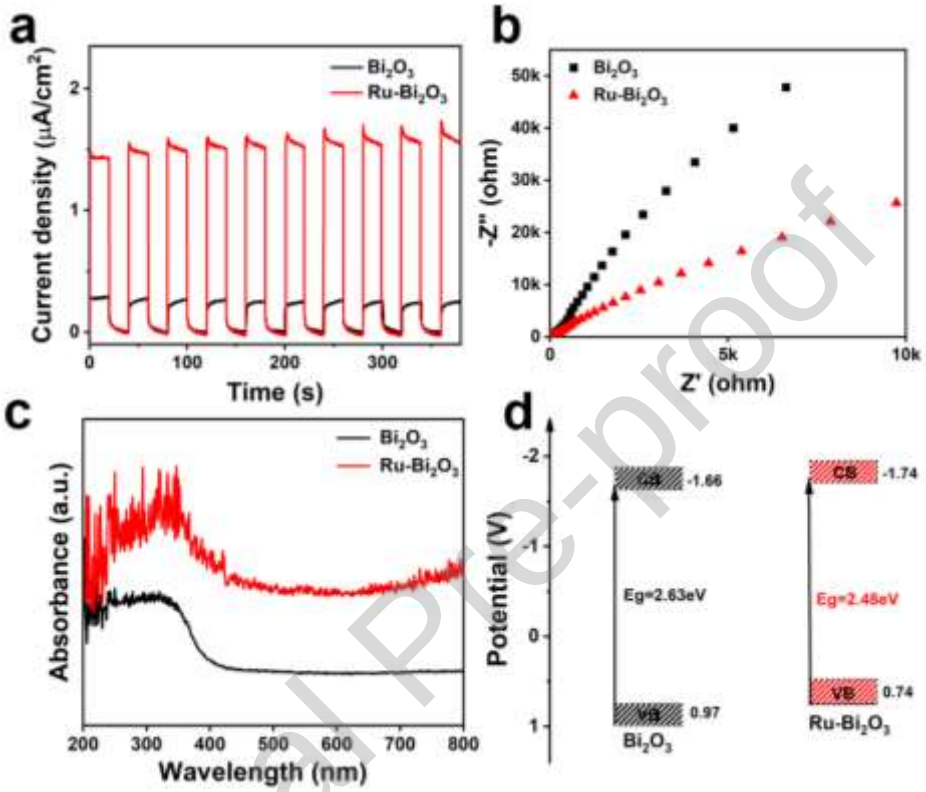

Fig. 4. (a) Photocurrent responses, (b) EIS, (c) DRS spectra, (d) Schematic band structure of Bi_2O_3 and Ru-Bi_2O_3.

3.4. Photocatalytic mechanism

DFT calculations were used to study the possible adsorption sites and electron transfer Firstly, the adsorption energies of Bi sites on Bi_2O_3, Bi sites on Bi_2O_3 with vacancies, and different Ru sites on Ru-Bi_2O_3 and Ru-Bi_2O_3 were calculated. It can be found that N_2 was difficult to adsorb on Bi_2O_3, and the possible individual sites of Ru on Bi_2O_3 were subsequently calculated (Fig. S10). From Fig. 5a, Ru site in Ru-Bi_2O_3 was the most effective adsorption site for N_2 in the bridge adsorption mode (Bi-O-Ru) in the presence of vacancies (ΔE = -1.03 eV). Besides, charge density difference analysis was performed to visualize the electron transfer behavior[51]. As shown in Fig. S11, significant charge accumulation (yellow) was observed around the Ru atoms, while significant charge depletion was observed around the other Bi and O elements in Ru-

Bi_2O_3(blue), suggesting that the electrons were transferred from Bi and O to Ru, and thus nitrogen easily adsorbed on the Ru sites and polarizes to NH_3. A Gibbs free energy model of the complete NRR pathway was developed to study the hydrogenation reaction pathway of N_2 on Ru-Bi_2O_3. As shown in Fig. 5b, it was found that the initial adsorption process of N_2 on Ru-Bi_2O_3 released 1.03 eV of energy and polarized the N_2 molecule by charge redistribution. The *N-N → *N-NH step was completely barrierless (from -1.03 to -1.48 eV). Meanwhile, the hydrogenation of *NNH had two processes, producing *NNH_2 (distal pathway) and *NHNH (alternate pathway). The free energy changes (ΔG) for forming NHNH* and NNH_2* from Ru-Bi_2O_3 were calculated to be 0.586 and 1.597 eV, respectively. Apparently, the NRR prefers to be hydrogenated via the binding alternation pathway of Ru-O-Bi, *N_2 → *NNH → *NHNH → *$NHNH_2$ → *NH_2NH_2 → NH_3. Meanwhile, the rate-limiting order is *N-NH → *NH-NH with a potential barrier of 0.58 eV (from -1.48 to -0.90 eV). The step *NH-*NH → *NH-NH_2 was also completely barrierless, and *NH-*NH_2 → *NH_2-NH_2 also occurred relatively easily(from -1.20 to -0.93 eV). The step *NH_2-NH_2 → *NH_2 was also easy, releasing 0.69 eV of free energy. The final *NH_2 → NH_3 step was energetically feasible. In addition, the integrated pathway for ammonia synthesis over Ru-Bi_2O_3 was exothermic with a released energy of -1.49 eV, thus exhibiting enhanced energy selectivity. In summary, Ru doping lowers the reaction barrier as well as the hydrogenation reaction potential, thereby promoting the promotion of N_2 chemisorption and activation. Thus, the significant enhancement of Ru-Bi_2O_3 activity was attributed to the sufficient supply of H*, which greatly contributes to the formation of ammonia.

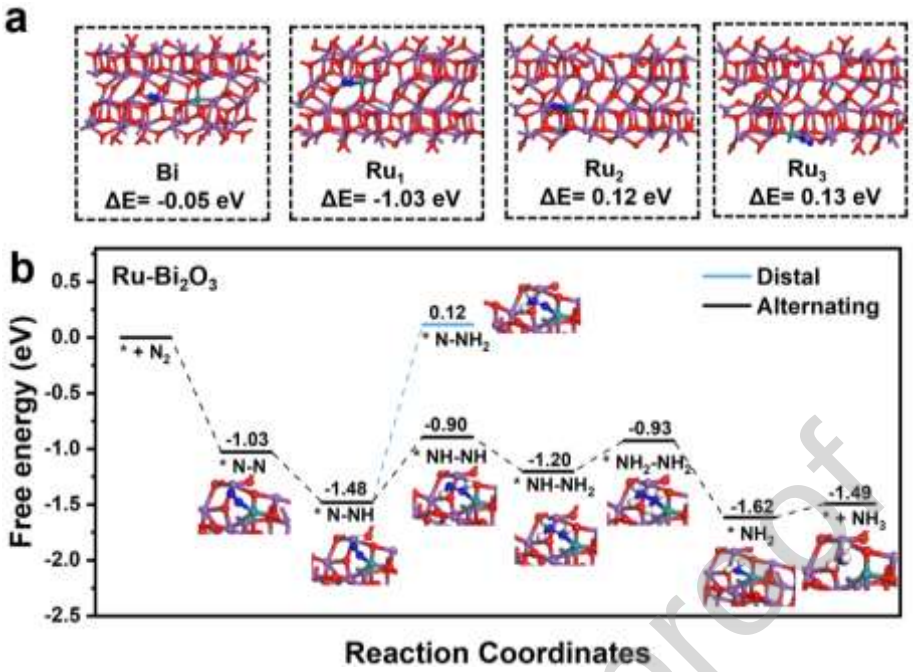

Fig.5. (a) N_2 adsorption energy at different sites on Ru-Bi_2O_3, (b) Free energy diagram of NRR on Bi_2O_3 and Ru-Bi_2O_3.

4. Conclusion

Ru-Bi_2O_3 with oxygen vacancies were prepared by impregnation and the rapid Joule heating method. Ru-Bi_2O_3 can suppress the recombination rate of photogenerated electron-hole pairs and enhance the nitrogen-fixing property by increasing the active site of nitrogen due to Ru doping. The oxygen vacancies formed by the rapid Joule heating method can effectively separate the photogenerated electron-hole pairs, which is conducive to N_2 adsorption. The optimal Ru-Bi_2O_3 photocatalytic nitrogen fixation rate was 32.9 μmol g^{-1} h^{-1} when the Ru content was 1.0 wt%. Gibbs free energy calculations by DFT revealed that the formation of Ru-O-Bi bonds on Ru-Bi_2O_3 as well as Ru sites was more favorable for N_2 adsorption and that the alternating nitrogen fixation mechanism was more favorable for nitrogen reduction. And the electron-rich structure favors ammonia formation. This research provides a new way for designing highly efficient photocatalysts under the rapid Joule heating method and offers new ideas for the rational design of catalytic sites for N_2 fixation by modulating the local electronic structure through metal doping.

Acknowledgments

This work was financially supported by Qingdao Natural Science Foundation (No.: 24-4-4-zrjj-195-jch). The authors thank Shiyanjia Lab (https://www.shiyanjia.com) for XRD analysis. The authors thank the e-Testing (https://www.eceshi.com) for XPS analysis.

References

1. Zhao, Z.; Ren, H.; Yang, D.; Han, Y.; Shi, J.; An, K.; Chen, Y.; Shi, Y.; Wang, W.; Tan, J.; Xin, X.; Zhang, Y.; Jiang, Z., Boosting Nitrogen Activation via Bimetallic Organic Frameworks for Photocatalytic Ammonia Synthesis. *ACS Catalysis* **2021,** *11* (15), 9986-9995.
2. Peng, Y.; Albero, J.; Franconetti, A.; Concepción, P.; García, H., Visible and NIR Light Assistance of the N_2 Reduction to NH_3 Catalyzed by Cs-promoted Ru Nanoparticles Supported on Strontium Titanate. *ACS Catalysis* **2022,** *12* (9), 4938-4946.
3. Kandemir, T.; Schuster, M. E.; Senyshyn, A.; Behrens, M.; Schlögl, R., The Haber–Bosch Process Revisited: On the Real Structure and Stability of "Ammonia Iron" under Working Conditions. *Angewandte Chemie International Edition* **2013,** *52* (48), 12723-12726.
4. Chen, L.-W.; Hao, Y.-C.; Guo, Y.; Zhang, Q.; Li, J.; Gao, W.-Y.; Ren, L.; Su, X.; Hu, L.; Zhang, N.; Li, S.; Feng, X.; Gu, L.; Zhang, Y.-W.; Yin, A.-X.; Wang, B., Metal–Organic Framework Membranes Encapsulating Gold Nanoparticles for Direct Plasmonic Photocatalytic Nitrogen Fixation. *Journal of the American Chemical Society* **2021,** *143* (15), 5727-5736.
5. Liu, H.; Wu, P.; Li, H.; Chen, Z.; Wang, L.; Zeng, X.; Zhu, Y.; Jiang, Y.; Liao, X.; Haynes, B. S.; Ye, J.; Stampfl, C.; Huang, J., Unravelling the effects of layered supports on Ru nanoparticles for enhancing N_2 reduction in photocatalytic ammonia synthesis. *Applied Catalysis B: Environmental* **2019,** *259*.
6. Li, Z.; Gao, Z.; Li, B.; Zhang, L.; Fu, R.; Li, Y.; Mu, X.; Li, L., Fe-Pt nanoclusters modified Mott-Schottky photocatalysts for enhanced ammonia synthesis at ambient conditions. *Applied Catalysis B: Environmental* **2020,** *262*.
7. Meng, S.-L.; Li, X.-B.; Tung, C.-H.; Wu, L.-Z., Nitrogenase inspired artificial photosynthetic nitrogen fixation. *Chem* **2021,** *7* (6), 1431-1450.
8. Shi, M.; Yang, H.; Zhao, Z.; Ren, G.; Meng, X., Bismuth-based semiconductors applied in photocatalytic reduction processes: fundamentals, advances and future perspectives. *Chemical Communications* **2023,** *59* (29), 4274-4287.
9. Yi, H.; Qin, L.; Huang, D.; Zeng, G.; Lai, C.; Liu, X.; Li, B.; Wang, H.; Zhou, C.; Huang, F.; Liu, S.; Guo, X., Nano-structured bismuth tungstate with controlled morphology: Fabrication, modification, environmental application and mechanism insight. *Chemical Engineering Journal* **2019,** *358*, 480-496.
10. Gao, X.; Shang, Y.; Liu, L.; Gao, K., Ag plasmon resonance promoted 2D AgBr-δ-Bi_2O_3 nanosheets with enhanced photocatalytic ability. *Journal of Alloys and Compounds* **2019,** *803*, 565-575.
11. Lv, C.; Zhong, L.; Yao, Y.; Liu, D.; Kong, Y.; Jin, X.; Fang, Z.; Xu, W.; Yan, C.;

Dinh, K. N.; Shao, M.; Song, L.; Chen, G.; Li, S.; Yan, Q.; Yu, G., Boosting Electrocatalytic Ammonia Production through Mimicking "π Back-Donation". *Chem* **2020,** *6* (10), 2690-2702.
12. Ren, G.; Zhao, Z.; Li, Z.; Zhang, Z.; Meng, X., Rapid Joule-Heating fabrication of oxygen vacancies and anchor of Ru clusters onto $BiVO_4$ for greatly enhanced photocatalytic N_2 fixation. *Journal of Catalysis* **2023,** *428*.
13. Bao, L.; Yuan, Y.-j.; Zhang, H.; Zhang, X.; Xu, G., Understanding the hierarchical behavior of Bi_2WO_6 with enhanced photocatalytic nitrogen fixation activity. *Dalton Transactions* **2021,** *50* (21), 7427-7432.
14. Ren, G.; Shi, M.; Li, Z.; Zhang, Z.; Meng, X., Electronic metal-support interaction via defective-induced platinum modified BiOBr for photocatalytic N_2 fixation. *Applied Catalysis B: Environmental* **2023,** *327*.
15. Liu, S.; Ren, G.; Gao, X.; Li, Z.; Wang, L.; Meng, X., A novel bismuth hydroxide ($Bi(OH)_3$) semiconductor with highly-efficient photocatalytic activity. *Chemical Communications* **2022,** *58* (59), 8198-8201.
16. Gao, X.; Xu, K.; He, H.; Liu, S.; Zhao, X., Oxygen vacancies – Cu doping junction control of δ-Bi_2O_3 nanosheets for enhanced photocatalytic nitrogen fixation. *Journal of Industrial and Engineering Chemistry* **2022,** *111*, 129-136.
17. Sudrajat, H.; Hartuti, S., Boosting electron population in δ-Bi_2O_3 through iron doping for improved photocatalytic activity. *Advanced Powder Technology* **2019,** *30* (5), 983-991.
18. Weber, M.; Rodriguez, R. D.; Zahn, D. R. T.; Stöwe, K.; Mehring, M., Polymorphism and Visible-Light-Driven Photocatalysis of Doped Bi_2O_3:M (M = S, Se, and Re). *Inorganic Chemistry* **2022,** *61* (3), 1571-1589.
19. Liu, G.; Li, S.; Lu, Y.; Zhang, J.; Feng, Z.; Li, C., Controllable synthesis of α-Bi_2O_3 and γ-Bi_2O_3 with high photocatalytic activity by α-Bi_2O_3→ γ-Bi_2O_3→ α-Bi_2O_3 transformation in a facile precipitation method. *Journal of Alloys and Compounds* **2016,** *689*, 787-799.
20. Zhang, Y.; Zhang, J.; Yi, Q.; Wang, F.; Fu, H.; Gao, H.; Liao, Y., In Situ Construction of Porous β-Bi_2O_3/BiOCOOH Heterojunction Photocatalysts: Enhancing Nitrogen Fixation Activity by the Synergistic Effect of Oxygen Vacancies and Lattice Oxygen. *ACS Applied Energy Materials* **2022,** *5* (8), 9503-9511.
21. Wang, B.; Liu, J.; Yao, S.; Liu, F.; Li, Y.; He, J.; Lin, Z.; Huang, F.; Liu, C.; Wang, M., Vacancy engineering in nanostructured semiconductors for enhancing photocatalysis. *Journal of Materials Chemistry A* **2021,** *9* (32), 17143-17172.
22. Wang, C.; Wang, S.; Ping, Y.; Zhao, Z.; Guo, D.; Wang, D.; Bu, X., Ru@MIL-125/MnO_x metal-organic-framework-based cocatalysts for photocatalytic nitrogen fixation. *Applied Catalysis B: Environment and Energy* **2024,** *347*.
23. Awati, A.; Maimaiti, H.; Wang, S.; Xu, B., Photo-derived fixation of dinitrogen into ammonia at ambient condition with water on ruthenium/coal-based carbon nanosheets. *Science of The Total Environment* **2019,** *695*.
24. Ren, G.; Shi, M.; Liu, S.; Li, Z.; Zhang, Z.; Meng, X., Molecular-level insight into photocatalytic reduction of N_2 over Ruthenium single atom modified TiO_2 by electronic Metal-support interaction. *Chemical Engineering Journal* **2023,** *454*.

25. Wang, B.-H.; Chen, G.-H.; Hu, B.; Chen, L.; Wang, X.; Tian, S.; Hu, X.-S.; Li, Y.; Peng, C.; Yin, S.-F., Recent advances in tunable metal–support interactions for enhancing the photocatalytic nitrogen reduction reaction. *EES Catalysis* **2024**.
26. Sun, J.-P.; Zhao, Z.; Li, J.; Li, Z.-Z.; Meng, X.-C., Recent advances in electrocatalytic seawater splitting. *Rare Metals* **2022,** *42* (3), 751-768.
27. Zhao, Z.; Ren, G.; Zhang, Z.; Meng, X.; Li, Z., Rapid Joule heating synthesis of Pt clusters on C_3N_4 with abundant nitrogen vacancies for highly-efficiently photocatalytic H_2 production. *Separation and Purification Technology* **2024,** *330*.
28. Sun, J.; Zhao, Z.; Li, Z.; Zhang, Z.; Zhang, R.; Meng, X., Ultrafast carbothermal shocking fabrication of cation vacancy-rich Mo doped Ru nanoparticles on carbon nanotubes for high-performance water/seawater electrolysis. *Journal of Materials Chemistry A* **2023,** *11* (41), 22430-22440.
29. Wulan, B.; Cao, X.; Tan, D.; Ma, J.; Zhang, J., To Stabilize Oxygen on In/In_2O_3 Heterostructure via Joule Heating for Efficient Electrocatalytic CO_2 Reduction. *Advanced Functional Materials* **2022,** *33* (1).
30. Wu, P.; Wang, T.; Xue, Q.; Wang, M.; Zhong, R.; Hu, J.; Chen, Z.; Wang, D.; Xue, G., Regulating Electronic Structure in Bi_2O_3 Architectures by Ti Mediation: A Strategy for Dual Active Sites Synergistically Promoting Photocatalytic Nitrogen Hydrogenation. *ChemSusChem* **2022,** *15* (11).
31. Long, Y.; Li, L.; Wang, S.; Chen, Y.; Wang, L.; Zhang, S.; Luo, L.; Jiang, F., Photocatalytic Removal of 17α-Ethinyl Estradiol Using the Bi_2O_3/Bi_2O_4 Photocatalyst. *Catalysis Letters* **2018,** *148* (12), 3608-3617.
32. Zhao, Z.; Ren, G.; Zhang, Z.; Meng, X.; Li, Z., Rapid Joule heating synthesis of Ni doped into porous honeycomb C_3N_4 with greatly improved photocatalytic H_2 production. *Inorganic Chemistry Frontiers* **2024,** *11* (9), 2634-2647.
33. Shang, H.; Wang, Y.; Jia, H.; Qu, M.; Ye, X.; Zhu, Q.; Zhang, D.; Wang, D.; Li, G.; Li, H., Constructing asymmetric active sites on defective Ru/$W_{18}O_{49}$ for photocatalytic nitrogen fixation. *Catalysis Science & Technology* **2023,** *13* (3), 854-861.
34. Pan, C.; Zhu, Y., A review of $BiPO_4$, a highly efficient oxyacid-type photocatalyst, used for environmental applications. *Catalysis Science & Technology* **2015,** *5* (6), 3071-3083.
35. Majhi, D.; Samal, P. K.; Das, K.; Gouda, S. K.; Bhoi, Y. P.; Mishra, B. G., α-NiS/Bi_2O_3 Nanocomposites for Enhanced Photocatalytic Degradation of Tramadol. *ACS Applied Nano Materials* **2018,** *2* (1), 395-407.
36. Wang, D.; Shen, H.; Guo, L.; Wang, C.; Fu, F.; Liang, Y., Ag/Bi_2MoO_{6-x} with enhanced visible-light-responsive photocatalytic activities via the synergistic effect of surface oxygen vacancies and surface plasmon. *Applied Surface Science* **2018,** *436*, 536-547.
37. Lv, Y.; Yao, W.; Zong, R.; Zhu, Y., Fabrication of Wide–Range–Visible Photocatalyst Bi_2WO_{6-x} nanoplates via Surface Oxygen Vacancies. *Scientific Reports* **2016,** *6* (1).
38. Yao, J. X.; Bao, D.; Zhang, Q.; Shi, M. M.; Wang, Y.; Gao, R.; Yan, J. M.; Jiang, Q., Tailoring Oxygen Vacancies of $BiVO_4$ toward Highly Efficient Noble‐Metal‐Free Electrocatalyst for Artificial N_2 Fixation under Ambient Conditions. *Small*

Methods **2018,** *3* (6).
39. Li, P.; Zhou, Z.; Wang, Q.; Guo, M.; Chen, S.; Low, J.; Long, R.; Liu, W.; Ding, P.; Wu, Y.; Xiong, Y., Visible-Light-Driven Nitrogen Fixation Catalyzed by Bi_5O_7Br Nanostructures: Enhanced Performance by Oxygen Vacancies. *Journal of the American Chemical Society* **2020,** *142* (28), 12430-12439.
40. Cai, Z.; Zhong, J.; Li, J.; Jin, H., Oxygen vacancies enriched BiOBr with boosted photocatalytic behaviors. *Inorganic Chemistry Communications* **2021,** *126*.
41. Liao, Y.; Lin, J.; Cui, B.; Xie, G.; Hu, S., Well-dispersed ultrasmall ruthenium on TiO_2(P25) for effective photocatalytic N2 fixation in ambient condition. *Journal of Photochemistry and Photobiology A: Chemistry* **2020,** *387*.
42. Wang, H.; Li, X.; Ruan, Q.; Tang, J., Ru and RuOxdecorated carbon nitride for efficient ammonia photosynthesis. *Nanoscale* **2020,** *12* (23), 12329-12335.
43. Maimaiti, H.; Wang, S.; Awati, A.; Xu, B., Photocatalytic synthesis of N_2/H_2O to ammonia on coal based GO/SiO_2 supported Ru composite catalyst. *Journal of Nanoparticle Research* **2020,** *22* (5).
44. Xia, S.; Zhang, G.; Gao, Z.; Meng, Y.; Xie, B.; Lu, H.; Ni, Z., 3D hollow Bi_2O_3@CoAl-LDHs direct Z-scheme heterostructure for visible-light-driven photocatalytic ammonia synthesis. *Journal of Colloid and Interface Science* **2021,** *604*, 798-809.
45. Xiao, C.; Wang, H.; Zhang, L.; Sun, S.; Wang, W., Enhanced Photocatalytic Nitrogen Fixation on MoO_2/BiOCl Composite. *ChemCatChem* **2019,** *11* (24), 6467-6472.
46. Wang, G.; Huo, T.; Deng, Q.; Yu, F.; Xia, Y.; Li, H.; Hou, W., Surface-layer bromine doping enhanced generation of surface oxygen vacancies in bismuth molybdate for efficient photocatalytic nitrogen fixation. *Applied Catalysis B: Environmental* **2022,** *310*.
47. Zhan, X.; Wang, H.; Zhou, G.; Chen, L.; Sun, Y.; Zhao, Y.; Liu, J.; Shi, H., Uracil-Doped Graphitic Carbon Nitride for Enhanced Photocatalytic Performance. *ACS Applied Materials & Interfaces* **2021,** *13* (10), 12118-12130.
48. Yu, H.; Chen, F.; Li, X.; Huang, H.; Zhang, Q.; Su, S.; Wang, K.; Mao, E.; Mei, B.; Mul, G.; Ma, T.; Zhang, Y., Synergy of ferroelectric polarization and oxygen vacancy to promote CO_2 photoreduction. *Nature Communications* **2021,** *12* (1).
49. Li, H.; Li, J.; Ai, Z.; Jia, F.; Zhang, L., Oxygen Vacancy‐Mediated Photocatalysis of BiOCl: Reactivity, Selectivity, and Perspectives. *Angewandte Chemie International Edition* **2017,** *57* (1), 122-138.
50. Yuan, J.; Yi, X.; Tang, Y.; Liu, M.; Liu, C., Efficient Photocatalytic Nitrogen Fixation: Enhanced Polarization, Activation, and Cleavage by Asymmetrical Electron Donation to N□N Bond. *Advanced Functional Materials* **2019,** *30* (4).
51. Ma, C.; Zhang, Y.; Yan, S.; Liu, B., Carbon-doped boron nitride nanosheets: A high-efficient electrocatalyst for ambient nitrogen reduction. *Applied Catalysis B: Environmental* **2022,** *315*.

Declaration of interests

☒ The authors declare that they have no known competing financial interests or personal relationships that could have appeared to influence the work reported in this paper.

Graphical abstract

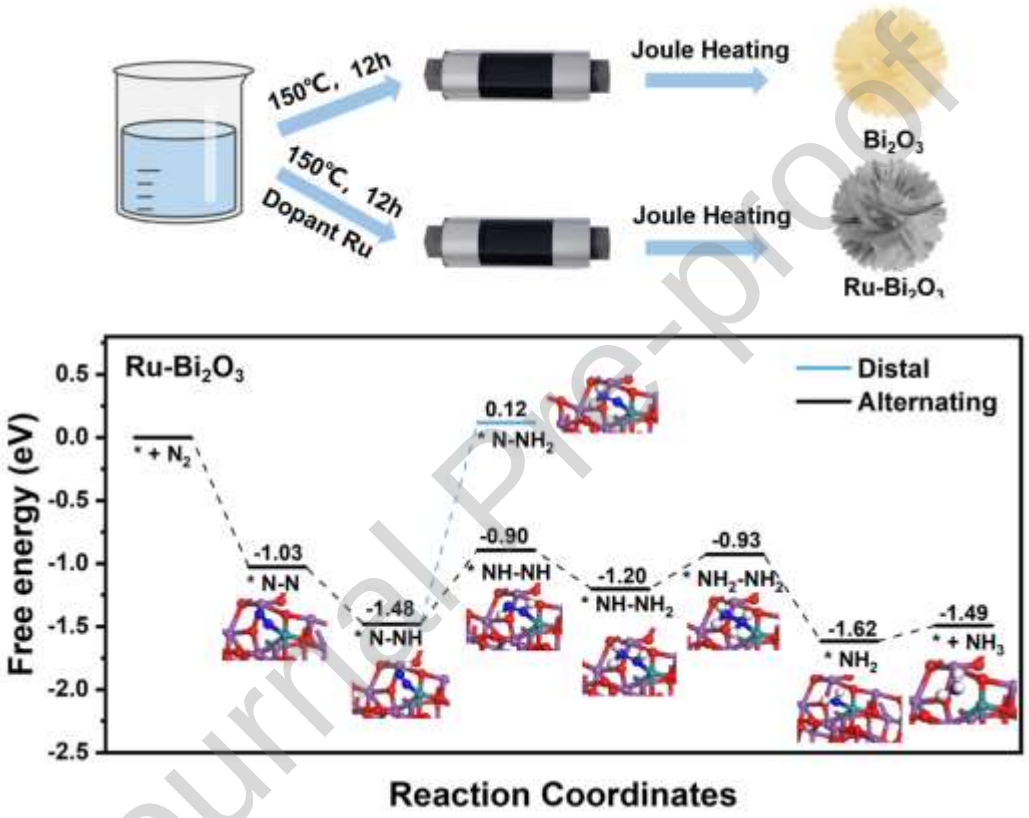

Highlights

- Preparation of Ru-Bi_2O_3 by fast Joule heating method
- The photocatalytic nitrogen fixation rate of Ru-Bi_2O_3 reached 32.9 μmol h^{-1} g^{-1}
- Doping of Ru and electron-rich bismuth state promote the activation of N_2.
- The photocatalytic reaction pathway were discussed.